Inorganic Chemistry
Article
pubs.acs.org/IC

Order–Disorder Transition and Weak Ferromagnetism in the Perovskite Metal Formate Frameworks of $[(CH_3)_2NH_2][M(HCOO)_3]$ and $[(CH_3)_2ND_2][M(HCOO)_3]$ (M = Ni, Mn)

Mirosław Mączka,* Anna Gągor, Bogusław Macalik, Adam Pikul, Maciej Ptak, and Jerzy Hanuza

Institute of Low Temperature and Structure Research, Polish Academy of Sciences, P.O. Box 1410, 50-950 Wrocław 2, Poland

S *Supporting Information*

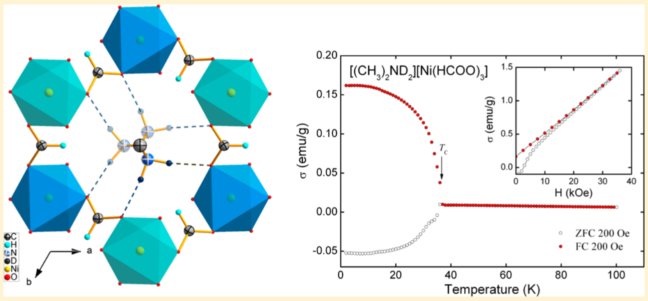

ABSTRACT: We report the synthesis, crystal structure, thermal, dielectric, Raman, infrared, and magnetic properties of hydrogen and deuterated divalent metal formates, $[(CH_3)_2NH_2][M(HCOO)_3]$ and $[(CH_3)_2ND_2][M(HCOO)_3]$, where M = Ni, Mn. On the basis of Raman and IR data, assignment of the observed modes to respective vibrations of atoms is proposed. The thermal studies show that for the Ni compounds deuteration leads to a decrease of the phase transition temperature T_c by 5.6 K, whereas it has a negligible effect on T_c in the Mn analogues. This behavior excludes the possibility of proton (deuteron) movement along the N–H···O (N–D···O) bonds as the microscopic origin of the first-order phase transition observed in these crystals below 190 K. According to single-crystal X-ray diffraction, the dimethylammonium (DMA) cations are dynamically disordered at room temperature, because the hydrogen bonds between the NH_2 (ND_2) groups and the metal-formate framework are disordered. The highly dynamic nature of hydrogen bonds in the high-temperature phases manifests in the Raman and IR spectra through very large bandwidth of modes involving vibrations of the NH_2 (ND_2) groups. The abrupt decrease in the bandwidth and shifts of modes near T_c signifies the ordering of hydrogen bonds and DMA^+ cations as well as significant distortion of the metal-formate framework across the phase transition. However, some amount of motion is retained by the DMA^+ cation in the ferroelectric phase and a complete freezing-in of this motion occurs below 100 K. The dielectric studies reveal pronounced dielectric dispersion that can be attributed to slow dynamics of large DMA^+ cations. The low-temperature studies also show that magnetic properties of the studied compounds can be explained assuming that they are ordered ferrimagnetically with nearly compensated magnetic moments of Ni and Mn. IR data reveal weak anomalies below 40 K that arise due to spin-phonon coupling. Our results also show that due to structural phase transition more significant distortion of the metal-formate framework occurs for the deuterated samples.

■ INTRODUCTION

Multiferroic materials present at least two coexisting orders among the electric, magnetic and elastic ones. The most interesting combination involves electric and magnetic orders since compounds where such orders coexists are potentially of great use in dynamic random access memories, data storage media, telecommunication systems, electromagnetic sensors, among others.[1] Because of these unique properties, the search for magnetoelectric compounds is of great technological and fundamental importance. Despite their usefulness, multiferroics are rare. These materials are mainly oxides of transition metal elements.[2] Another example is the class of metal–organic frameworks (MOFs) with the formula $[(CH_3)_2NH_2][M(HCOO_3)_3]$, which closely resemble pure inorganic multiferroic $BiFeO_3$ with perovskite ABO_3-type structures in which A is the dimethylammonium (DMA^+) cation, the B is the divalent metal ion, and the anion O is replaced by formate.[3−10]

Wang et al. have reported that MOFs of formula $[(CH_3)_2NH_2][M(HCOO)_3]$ with M = Mn, Ni, Co show magnetic ordering at 8–36 K.[4] Later, Jain et al. and Guo et al. reported electric ordering in $[(CH_3)_2NH_2][M(HCOO)_3]$ with M = Zn, Mn, Ni, Co, Fe at 160–185 K,[5] and the observation of the good dielectric hysteresis loop for $[(CD_3)_2ND_2][Co(DCOO)_3]$ below T_c by Fu et al. confirmed that the low temperature structure of these materials is ferroelectric.[6] Very recently, it has been reported that magnetoelectric coupling exists in $[(CH_3)_2NH_2][Mn(HCOO)_3]$ already in the paramagnetic state below the ferroelectric phase transition T_c = 185 K.[7] This discovery could open up new routes to designing various MOFs exhibiting high-temperature sensitive magnetoelectric effects.[7] It is worth to add that nonmagnetic $[(CH_3)_2NH_2][Zn(HCOO)_3]$ has also been shown to exhibit a glassy behavior at low temperatures.[8]

Single-crystal X-ray diffraction data showed that these compounds crystallize in the trigonal space group $R\bar{3}c$, with the disordered DMA^+ cations located in the cages of the network.[4,5] The onset of ferroelectricity at low temperatures

Received: September 25, 2013
Published: December 9, 2013

dx.doi.org/10.1021/ic402425n | *Inorg. Chem.* 2014, 53, 457−467

has been associated to partial (in the case of $[(CD_3)_2ND_2][Co(DCOO)_3]$) or full (in the case of $[(CH_3)_2NH_2][Mn(HCOO)_3]$) ordering of the DMA^+ cations, associated with the decrease of symmetry to *Cc*, but a detailed mechanism of the phase transition is still not fully understood.[6,8−10] In particular, conventional X-ray diffraction methods cannot yield the hydrogen (deuterium) atoms positions, which is the major drawback for interpreting the phase transition mechanism that rely on H-bond or D-bond type close contacts. In contrast, spectroscopy is site sensitive and thus is a good probe for local structure with high spatial resolution. Under these circumstances, vibrational spectroscopic techniques offer numerous advantages since they are particularly suited to studies of H-bonds as well as order−disorder phase transitions associated with motions of hydrogen or deuterium atoms. Replacement of a hydrogen atom by a deuterium atom also helps to locate all vibrational modes that involve strong contribution of hydrogen (deuterium) atom motions. Raman and infrared (IR) spectroscopies are also known to be powerful probes for studying spin−phonon interactions in magnetic materials.[2,11] It is therefore important and interesting to study deuterated MOFs to see how deuteration affects T_c, the dielectric constant, and vibrational spectra.

In this work, we report synthesis and study of $[(CH_3)_2NH_2][Mn(HCOO)_3]$ (DMMn), $[(CH_3)_2NH_2][Ni(HCOO)_3]$ (DMNi), $[(CH_3)_2ND_2][Mn(HCOO)_3]$ (DMMnD), and $[(CH_3)_2ND_2][Ni(HCOO)_3]$ (DMNiD). These formates are characterized by single crystal X-ray diffraction (XRD), differential scanning calorimetry (DSC), dielectric anomaly, measurements of low temperature magnetization, Raman scattering, and IR spectroscopy in order to understand the nature of the observed vibrational modes and obtain deeper insight into the microscopic mechanism of the ferroelectric phase transition in these MOFs as well as spin−phonon coupling due to magnetic ordering at very low temperatures.

■ EXPERIMENTAL SECTION

Synthesis. $MnCl_2$ (99%, Aldrich), $NiCl_2$ (98%, Aldrich), *N*,*N*-dimethylformamide (DMF) (99.8%, Aldrich), and D_2O (Aldrich) were commercially available and used without further purification. All crystals were prepared under solvothermal conditions at 140 °C. In a typical experiment, a mixture of MCl_2 (5 mmol), DMF (30 mL), and H_2O or D_2O (30 mL) was heated in a Teflon-lined microwave autoclave for 48 h. Block crystals (light-pink for Mn and green for Ni) were obtained by evaporating the solution at room temperature for 5 days. The crystals were filtered from the mother liquid and washed by ethanol. The yield is about 60% based on the starting metal salts. A good match of their powder XRD patterns confirmed the phase purity of obtained crystals with a simulation from the single-crystal structure determination (see Figure S1 in the Supporting Information).

Crystallographic Structure Determination. Single-crystal diffraction data were collected at 295 K on a KM4-CCD diffractometer operating in κ geometry. The graphite monochromated Mo Kα radiation was used. Intensities were measured in ω-scan mode with $\Delta\omega = 1.0°$ using the CrysAlis CCD program. The CrysAlis. RED software version 1.170.32 (Oxford Diffraction) was used for data processing. An empirical absorption correction was applied using spherical harmonics implemented in Scale3 Abspack scaling algorithm. The structure was refined by full-matrix least-squares method by means of the SHELX-97 program package. Because of the disorder of $(CH_3)_2ND_2^+$ and $(CH_3)_2NH_2^+$ counterions the nitrogen atoms were refined isotropically. Hydrogen as well as deuterium atoms were included in geometric positions (C−H 0.95 Å) and treated as riding atoms. The $U_{iso}(H)$ values were constrained to be $1.2U_{eq}$(carrier atom).

In addition, powder XRD pattern was obtained for all samples on an X′Pert PRO X-ray diffraction system equipped with a PIXcel ultrafast line detector, focusing mirror, and Soller slits for Cu Kα_1 radiation (λ = 1.54056 Å).

DSC. The DSC measurements of obtained crystals were performed in the temperature range of 100−350 K on a DSC-7 instrument (Perkin-Elmer) at a rate of 10 °C/min under a nitrogen atmosphere with two cycles. Fresh crystalline powdered samples of 19.2 mg (for DMMn), 17.6 mg (for DMMnD), 3.9 mg (for DMNi), and 7.1 mg (for DMNiD) were used.

Dielectric Properties. The complex dielectric permittivity was measured for DMNi and DMNiD at a frequency range from 10^0 to 10^6 Hz using a broadband impedance Alpha analyzer with Active Sample Cell (Novocontrol). The measurements were taken every 1 deg over the temperature range from 90 to 373 K. Since the obtained single crystals were not big enough to perform single crystal dielectric measurements, pellets made of well-dried samples were measured instead. The pellets with a diameter of 6 mm and thickness of 0.6 mm were located between gold electrodes with a diameter of 6 mm. The samples were located in the sample chamber filled by dry nitrogen. The temperature values, with a stability ±0.2 K, were changed by flow of vaporized liquid nitrogen heated and controlled by a self-made heating system.

The complex dielectric function is given by $\varepsilon''(\omega) = \varepsilon' - i\varepsilon'' = -i/(\omega Z^*(\omega)C_0)$ where Z^* is the measured complex impedance, C_0 is the geometrical capacitance of the sample, and $\omega = 2\pi f$ is the angular frequency. All measurements including the calibration routine, temperature stabilization, and data acquisition were automatically controlled.

Raman and IR Studies. Raman spectra were measured using a Bruker FT 100/S spectrometer with YAG:Nd laser excitation (1064 nm) and a helium-flow Oxford cryostat. Temperature-dependent IR spectra were measured for the sample in KBr pellet in the range of 3800−400 cm^{-1} and in Apiezon N suspension in the range of 500−50 cm^{-1} with the Biorad 575C FT-IR spectrometer using a helium-flow Oxford cryostat. The resolution was 2 cm^{-1}.

■ RESULTS AND DISCUSSION

Thermal Properties. The DSC measurements show a heat anomaly at 187.0 K upon warming and 181.0 K upon cooling for DMMn (Figure S2, Supporting Information). The 187.0 K phase transition temperature upon heating is in very good agreement with the DSC data reported in the literature.[10] The nearly symmetric shape of this anomaly and the relatively large thermal hysteresis of 6 K indicates a reversible, first-order phase transition. The DSC data for DMMnD show a very similar heat anomaly at 187.5 K upon heating and 180.3 K upon cooling. As can be noticed, the isotope effect for the Mn compound is very small. Similar behavior was reported for $[(CH_3)_2NH_2][Co(HCOO)_3]$ and its perdeutero analogue $[(CD_3)_2ND_2][Mn(DCOO)_3]$, for which $\Delta T_c \approx 1$ K.[6] The DSC data for DMNi (DMNiD) show a heat anomaly at 178.7 K (173.1 K) upon warming and 171.9 K (166.3 K) upon cooling. These anomalies are less sharp than those observed for DMMn and DMMnD, but the observed thermal hysteresis is also relatively large (about 6 K), indicating a first-order phase transition. Interestingly, in the case of the Ni-compounds, the isotopic effect is clearly observed; that is, T_c decreases by 5.6 K after deuteration. It is well-known that most of the H-bonded ferroelectrics, especially those belonging to the KDP type (KH_2PO_4, $NH_4H_2PO_4$, etc.), show large upward shifts of their lower T_c when D is substituted for H. This behavior is related to the ordering of protons in the hydrogen bonds, and to account for this large isotopic effect the tunneling proton model was introduced.[12] However, there are some instances where T_c is weakly affected by deuteration. For instance, in $LiNH_4SO_4$

for which the phase transition mechanism is associated mainly with transition into a state of free rotation of NH_4^+ ions at high temperatures, the T_c increased only by 4.5 K upon deuteration.[13] On the other hand, for purely order−disorder phase transition in KNO_3, the ^{15}N-enriched KNO_3 showed a slight decrease of T_c when compared to the natural ^{14}N isotope.[14] The very weak H-atom isotopic effect for DMMn and negative effect for DMNi exclude the possibility of proton (deuteron) movement along N−H···O (N−D···O) bonds as the microscopic origin of the first-order phase transition in these MOF.

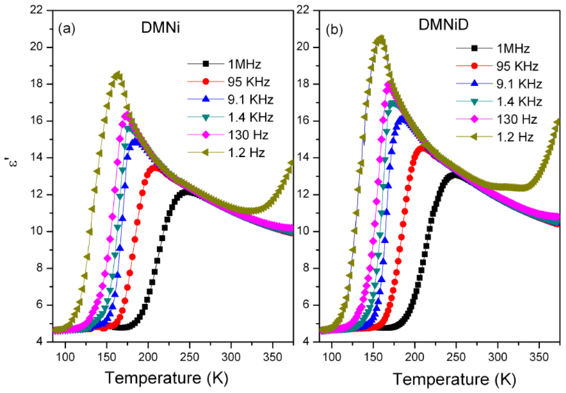

Figure 1. The real part of the complex dielectric constant of (a) DMNi and (b) DMNiD measured at different frequencies.

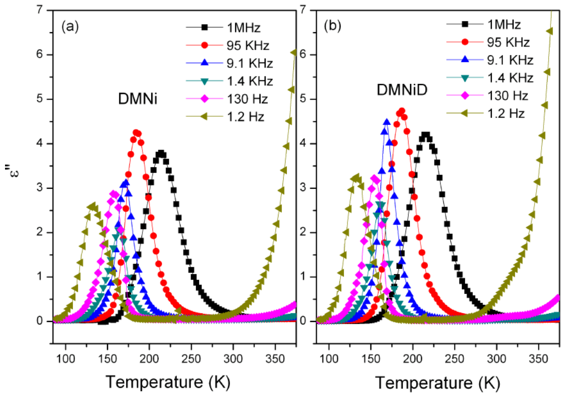

Figure 2. The imaginary part of the complex dielectric constant of (a) DMNi and (b) DMNiD measured at different frequencies.

Dielectric Properties. The temperature dependences of real (ε') and imaginary (ε'') part of the complex dielectric function as a function of frequency for DMNi and DMNiD are presented in Figures 1 and 2. The real part ε' displays a broad peak at 164 K (158 K) at 1.2 Hz and at 242 K (244 K) at 1 MHz for DMNi (DMNiD). The reciprocal ε' data at 1.2 Hz show that the Curie−Weiss Law holds in the paraelectric phase near T_c (see Figure S3a, Supporting Information). The Curie−Weiss constant $C \approx 1.5 \times 10^3$ and 1.7×10^3 for DMNi and DMNiD, respectively. As can be noticed, ε' diminishes with increasing frequency, and the imaginary part ε'' exhibits a broad peak just where the ε' increases most steeply (Figures 1 and 2). This observation is characteristic of the Debye-type dielectric relaxation, in which the reorientation of dipoles cannot respond to the applied ac electric field with high frequency exceeding a relaxation rate $1/\tau$. This mechanism is expressed as

$$\varepsilon'(\omega) = \frac{\varepsilon_0 - \varepsilon_\infty}{1 + \omega^2\tau^2}\varepsilon_\infty \tag{1}$$

$$\varepsilon''(\omega) = \frac{(\varepsilon_0 - \varepsilon_\infty)\omega\tau}{1 + \omega^2\tau^2} \tag{2}$$

where τ, ω, ε_0, and ε_∞ are the relaxation time, frequency, static dielectric constant, and high-frequency dielectric constant, respectively. The ε' peak exhibits very large relaxation, with a difference of approximately 78 K (86 K) for DMNi (DMNiD) from low to high frequencies. It should be noticed that a sharp maximum in the temperature dependence of the ε', which can be attributed to the onset of the ferroelectric phase transition, is clearly seen only at very low frequencies, implying extremely slow dynamics of polarization. Our data also show that at low frequencies the maximum of the ε' is observed at about 5 K lower temperature for DMNiD, when compared to DMNi (see in Figure S4, Supporting Information). The shift of the maximum toward a lower temperature for the deuterated sample is consistent with the DSC data showing a lower phase transition temperature for this sample. The Cole−Cole diagram (Figure 3) exhibits semicircles for temperatures above T_c, representing the Debye-type dielectric relaxation with a single relaxation. On the other hand, more relaxation mechanisms are noted by a complicated curve below T_c. The relaxation time, obtained from fitting data to eq 2 for temperatures above T_c, shows that it is proportional to temperature near T_c (see Figure S3b).

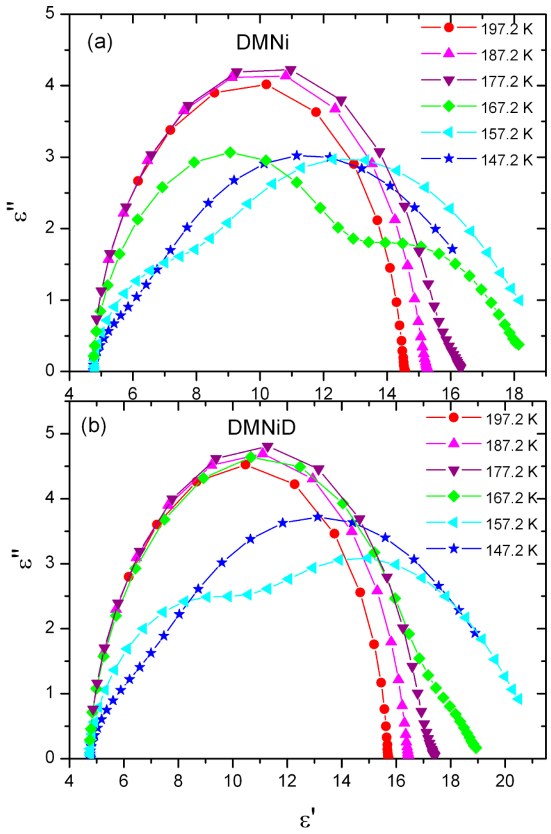

Figure 3. The Cole−Cole diagram of (a) DMNi and (b) DMNiD at a few temperatures.

It has recently been suggested that the phase transition in $[(CH_3)_2NH_2][M(HCOO)_3]$ compounds may be associated with improper ferroelectric characteristics.[15] At improper ferroelectric transition, the small spontaneous polarization appears only as a secondary effect due to a coupling with a primary order parameter. The transition is connected only with a small dielectric anomaly, and no Curie−Weiss Law is expected to hold.[16] Improper ferroelectrics have $C \approx 10$ and for order−disorder ferroelectrics $C \approx 10^3$.[15] Although the compounds studied here exhibit weak dielectric anomalies, the Curie−Weiss Law holds and the value of the C constant is typical as for many other order−disorder ferroelectrics. Our results show, therefore, that the phase transition reported here can be attributed to the dynamics of DMA^+ cations inside the cavities. In the paraelectric phase, the DMA^+ cations are disordered, and we may suppose that the hopping motion of these cations between three orientations is responsible for the dielectric dispersion. Ordering of these large cations causes the phase transition, and the rotation of the DMA^+ cations gradually slows down until it freezes completely at low temperatures. Slow dynamics of polarization can be attributed to the large size of the DMA^+ cation, as observed previously for $(CH_3)_2NH_2Al(SO_4)_2{\cdot}6H_2O$, for which the relaxation time reached at T_c = 152 K the value $\tau = 1.6 \times 10^{-7}$ s.[17] Weak changes upon deuteration are also consistent with the hopping motion of DMA^+ cations as a cause of the dielectric dispersion and the phase transition mechanism based on ordering of these cations.

Magnetic Properties. Figures 4 and 5 present temperature dependences of the magnetization of DMNiD and DMMnD, respectively, measured in the zero-field cooling (ZFC) and field cooling (FC) regimes. In the FC regime, distinct Brillouin-like-shaped anomalies in the $\sigma(T)$ curves manifest ferromagnetic-like phase transitions at T_C = 37 K (DMNiD) and 8.5 K (DMMnD), accompanied with a nearly mirror-like behavior of the ZFC curves. As can be inferred from the inset to Figures 4 and 5, these magnetic hystereses are visible only in low external magnetic fields (much less than 20 kOe in DMNiD and 1 kOe in DMMnD). At higher fields, the $\sigma(H)$ curves show linear behavior, which is characteristic of paramagnets. The latter observation is in line with the fact that at high fields both compounds exhibit Curie-like paramagnetism in $\sigma(T)$.

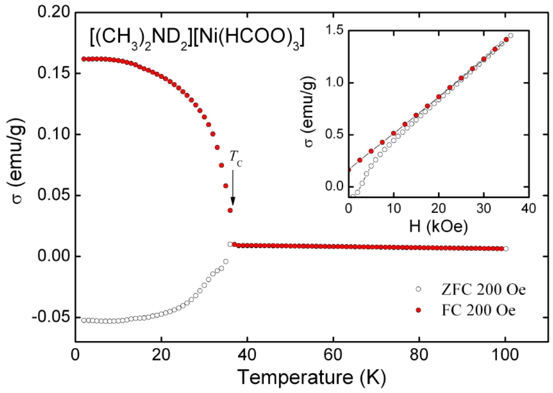

Figure 4. Temperature dependence of the magnetization of DMNiD measured at 200 Oe in the zero-field cooling (ZFC) and field cooling (FC) regimes. Inset: hysteresis loop of DMNiD measured at 1.7 K.

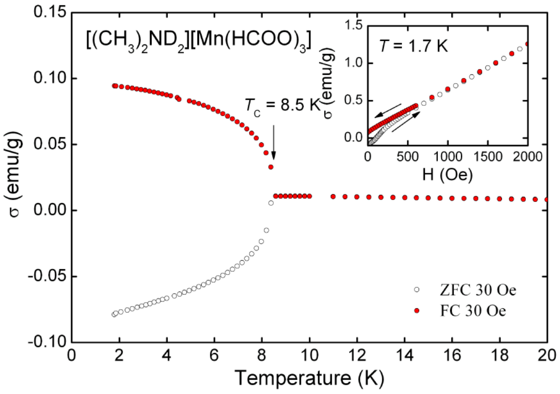

Figure 5. Temperature dependence of the magnetization of DMMnD measured at 30 Oe in the zero-field cooling (ZFC) and field cooling (FC) regimes. Inset: hysteresis loop of DMMnD measured at 1.7 K.

The spontaneous magnetization in the FC measurement is achieved at the lowest temperature studied, that is, 1.7 K, about 0.16 emu/g in 200 Oe for DMNiD and 0.095 emu/g in 30 Oe for DMMnD, which in the case of all the magnetic moments aligned to the external magnetic field would correspond to only 6.9×10^{-3} and 4.0×10^{-3} μ_B/f.u., respectively. These values are as much as 3 orders of magnitude lower than the expected Hund's-rules-based values calculated for free Ni^{2+} and Mn^{2+} ions with the orbital quenching assumed (i.e., 2.83 and 5.92 μ_B, respectively).

All the described above features of the compounds studied can be explained assuming that they are ordered ferrimagnetically with nearly compensated magnetic moments of Ni and Mn. Such a scenario was proposed, for example, for a canted antiferromagnet $Ni(HCOO)_2{\cdot}2H_2O$, which exhibits somehow similar magnetic behavior: weak ferromagnetism at low fields and distinct Curie-like paramagnetism in high fields.[18]

Structural Studies. The details of data collection, cell, and refinement parameters for DMMnD, DMMn, DMNiD, and DMNi at 298 K are summarized in Table S1, Supporting Information. The crystal structure of both deuterated DMMnD and DMNiD crystals is isomorphic to its hydrogen analogues (see Table S1). The rigid, three-dimensional pseudoperovskite substructure (consisting of trigonally distorted MnO_6 (NiO_6) octahedra which are connected by formate groups) accommodates $(CH_3)_2ND_2^+$ cations in the large cavities. Despite the fact that cations interact with formate oxygen atoms via H-bonds, with a donor to acceptor (D···A) distance of 2.904(4) Å in DMNiD and 2.929(5) Å in DMMnD, they are not able to overcome thermally activated motions and, as a result, rotate around a 3-fold axis (Figure 6a). Three equivalent positions of $(CH_3)_2ND_2^+$ give six possible equivalent H-bonds Figure 6b), and none of them are favored. At low temperatures the rotations should be frozen. Two possible scenarios may happen. Structural distortion of the rigid anionic substructure may break the 3-fold symmetry and introduce a favored position for $(CH_3)_2ND_2^+$. This phase transition should form crystal domains with ordered or more ordered substructure of cations. In the case of a lack of distortion, the cations may statistically occupy one of the three equivalent positions around a 3-fold axis. Dynamical disorder should evolve into a statistical one without formation of a domain structure.

After deuteration of amine groups, the crystal structure does not change much. Distances and angles for non-hydrogen atoms are very similar compared to nondeuterated crystals. One of the expected isotopic effects is weakening of H-bonds resulting from a deuterium shift toward the donor atom. This so-called Ubbelohde effect is observed for most strong O−H···O bridges that elongate upon replacing H with D. However, for moderate and weak H-bonds, negligible or even negative Ubbelohde effect may appear.[19] The discrete changes of the H-

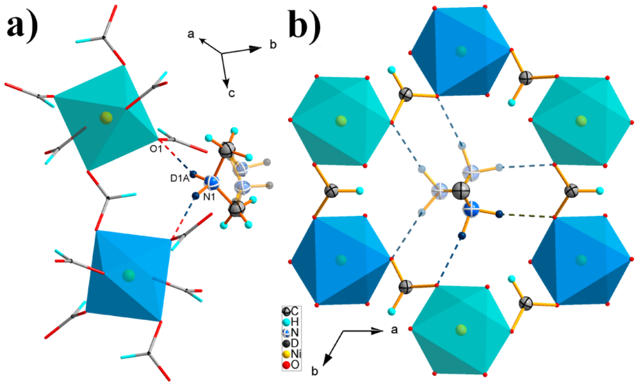

Figure 6. (a) Possible N–D···O H-bonds between $(CH_3)_2ND_2^+$ cations and rigid $M(HCOO)_3^-$ groups; D···A distance is equal to 2.928(5) Å and 2.904(4) Å in DMMnD and DMNiD analogues, respectively; equivalent positions of $(CH_3)_2ND_2^+$ cations are made transparent. (b) Distribution of $(CH_3)_2ND_2^+$ cations around trigonal 3 axis in the crystal cages. Equivalent H-bonds are marked as dashed lines. Dark polyhedrons are on the bottom, brighter above the plane intersecting positions of ND_2 groups.

bond geometries in the studied crystals are shielded by the disorder of $(CH_3)_2ND_2^+$ and $(CH_3)_2NH_2^+$ cations. The disorder of molecules introduces dispersed electron density, which disables the accurate estimation of hydrogen and deuterium positions and accurate validation of bond distances and angles. In deuterated crystals, the intermolecular distances between donor and acceptor atoms are very similar compared to its hydrogen analogues. The D···A distance changes after deuteration from 2.920(4) Å in DMMn to 2.929(5) Å in DMMnD and from 2.913(3) Å in DMNi to 2.904(4) Å in DMNiD. Table 1 shows the idealized geometry of H-bonds (D-bonds) and weak N–H···O (N–D···O) contacts in deuterated and nondeuterated crystals.

Table 1. Geometries of the N–H···O and N–D···O Bonds between the DMA$^+$ Cations and the Anionic Framework[a]

D–H···A	D···H	H···A	D···A	∠DHA
		DMMn		
N1–H1A···O1	0.97	1.99	2.920(4)	159.1
N1–H1B···O1	0.97	1.99	2.920(4)	159.1
N1–H1A···O1	0.97	2.61	3.2803(13)	126.5
N1–H1B···O1	0.97	2.61	3.2803(13)	126.5
		DMMnD		
N1–D1A···O1	0.98	1.99	2.929(5)	159.0
N1–D1B···O1	0.98	1.99	2.929(5)	159.0
N1–D1A···O1	0.98	2.61	3.2853(14)	126.1
N1–D1B···O1	0.98	2.61	3.2853(14)	126.1
		DMNi		
N1–H1A···O1	0.96	2.00	2.913(3)	159.3
N1–H1B···O1	0.96	2.00	2.913(3)	159.4
N1–H1A···O1	0.96	2.60	3.2651(11)	126.5
N1–H1B···O1	0.96	2.60	3.2651(11)	126.6
		DMNiD		
N1–D1A···O1	0.96	1.99	2.904(4)	159.3
N1–D1B···O1	0.96	1.99	2.904(4)	159.3
N1–D1A···O1	0.96	2.60	3.2548(12)	126.4
N1–D1B···O1	0.96	2.60	3.2548(12)	126.4

[a] Distances, Å; angles, °.

Vibrational Studies. The vibrational spectra of the studied compounds may be understood by dividing **k** = 0 vibrations into internal vibrations of the DMA$^+$ and formate ions, and the lattice vibrations. Free $HCOO^-$ ion has C_{2v} symmetry, and its fundamental internal vibrations consist of the C–H stretching mode ν_1, the symmetric C–O stretching mode ν_2, the antisymmetric C–O stretching mode ν_4, the symmetric O–C–O bending (scissor) mode ν_3, the C–H in-plane bending mode ν_5, and the C–H out-of-plane bending mode ν_6.[20] Since both the room temperature phase (space group $R\bar{3}c$) and low-temperature phase (space group Cc) comprise six $HCOO^-$ ions in the primitive cell, the number of internal of $HCOO^-$ modes increases to 36, as presented in Table S2, Supporting Information. Free DMA$^+$ cation also has C_{2v} symmetry and the 27 internal modes are distributed among the irreducible representation: $\Gamma = 9A_1 + 5A_2 + 7B_1 + 6B_2$.[21] Of these modes, the nine skeletal modes of H_2NC_2 correspond to $\Gamma = 4A_1 + A_2 + 2B_1 + 2B_2$,and they can be subdivided into symmetric stretching ($\nu_s(NH_2)$), antisymmetric stretching (($\nu_{as}(NH_2)$), scissoring ($\delta(NH_2)$), rocking ($\rho(NH_2)$), wagging ($\omega(NH_2)$), and torsion or twisting ($\tau(NH_2)$) modes of the NH_2 group as well as symmetric stretching ($\nu_s(CNC)$), antisymmetric stretching ($\nu_{as}(CNC)$), and bending ($\delta(CNC)$) modes of the CNC group. The remaining 18 degrees of freedom correspond to the modes of two methyl groups. These modes can be subdivided into symmetric stretching ($\nu_s(CH_3)$), antisymmetric stretching (($\nu_{as}(CH_3)$), bending ($\delta(CH_3)$), rocking ($\rho(CH_3)$), and torsion ($\tau(CH_3)$) modes. Since the NH_2 group of the DMA$^+$ cations is disordered in the $R\bar{3}c$ phase, we do not present distribution of the internal modes of the NH_2 group and lattice modes of DMA$^+$ among the irreducible representation for this structure. However, we present the number of these modes calculated under the assumption that the site symmetry of DMA$^+$ in the $R\bar{3}c$ phase is C_2 (see Table S2, Supporting Information). This approximation is reasonable since according to the XRD data, the nitrogen atom is located on 2-fold axis. For the ordered Cc structure, the complete correlation diagram is presented (see Table S2).

The Raman and IR spectra of the studied compounds are presented in Figures 7, 8, and S5–S10, Supporting Information. The observed IR and Raman frequencies (in cm^{-1}) are listed in Tables S3 and S4, Supporting Information together with suggested assignments that were mostly based on literature data.[4,20,22,23] It is worth noting, however, that the assignment of some other modes, especially those related to the NH_2 (ND_2) group, was obtained by comparison of the spectra for the hydrogen and deuterated samples. For instance, this comparison shows that the Raman bands at 3049 and 3040 cm^{-1} are not affected by the deuteration (see Figures 7 and S5). It is, therefore, clear that they do not correspond to the NH_2 group, as suggested by Sanchez-Andujar et al.[10] but should be assigned to stretching modes of the CH_3 groups. On the other hand, the bands at 2786 and 2798 cm^{-1}, which appear in the Raman spectra of DMMn at low temperatures but are absent in the Raman spectra of DMMnD, can be unambiguously assigned to stretching modes of the NH_2 group. Here it is important to mention that for DMMn and DMNi, only two $\nu_3(HCOO^-)$ modes are observed at 5 K in the 790–830 cm^{-1} region, but the number of bands in this spectral range increases to three (four) for DMMnD (DMNiD) (see Figures 8 and S6–S8, Supporting Information). An additional band appears also near 770 cm^{-1}. Moreover, upon deuteration the $\nu_3(HCOO^-)$ modes shift slightly toward higher frequencies. For instance, the bands

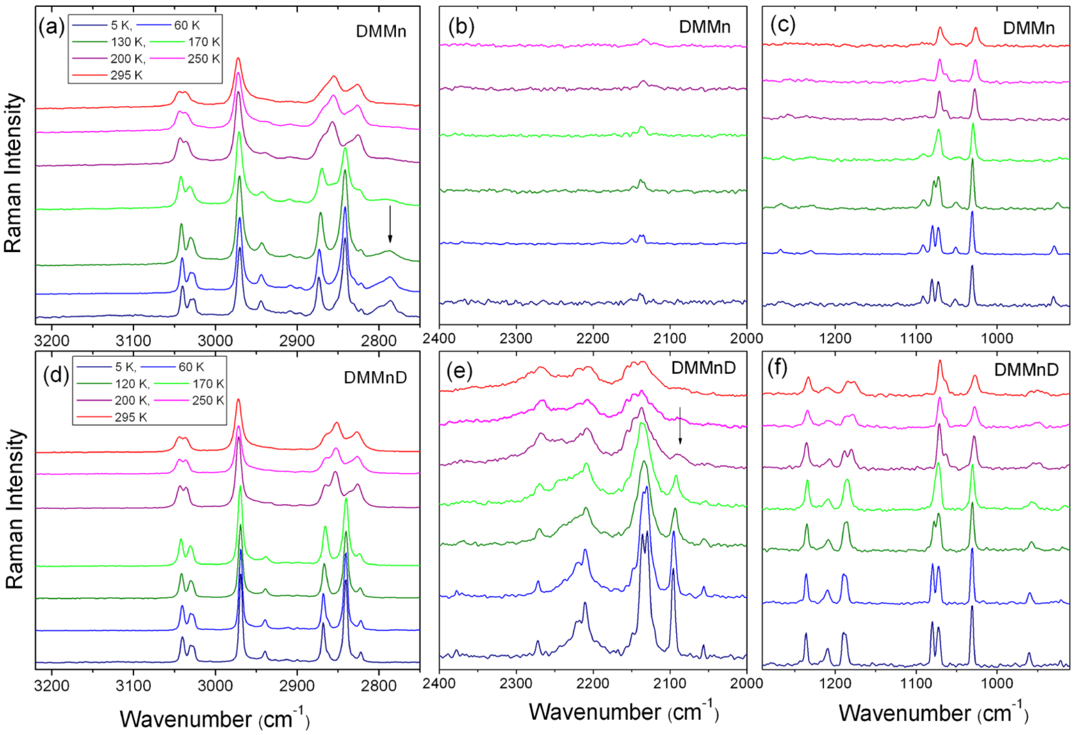

Figure 7. Detail of the Raman spectra results corresponding to the spectral ranges 2750−3320, 2000−2400, and 910−1290 cm^{-1} for DMMn ((a), (b), and (c)) and DMMnD ((d), (e), and (f)). Arrows indicate the bands that exhibit a pronounced increase in intensity upon cooling.

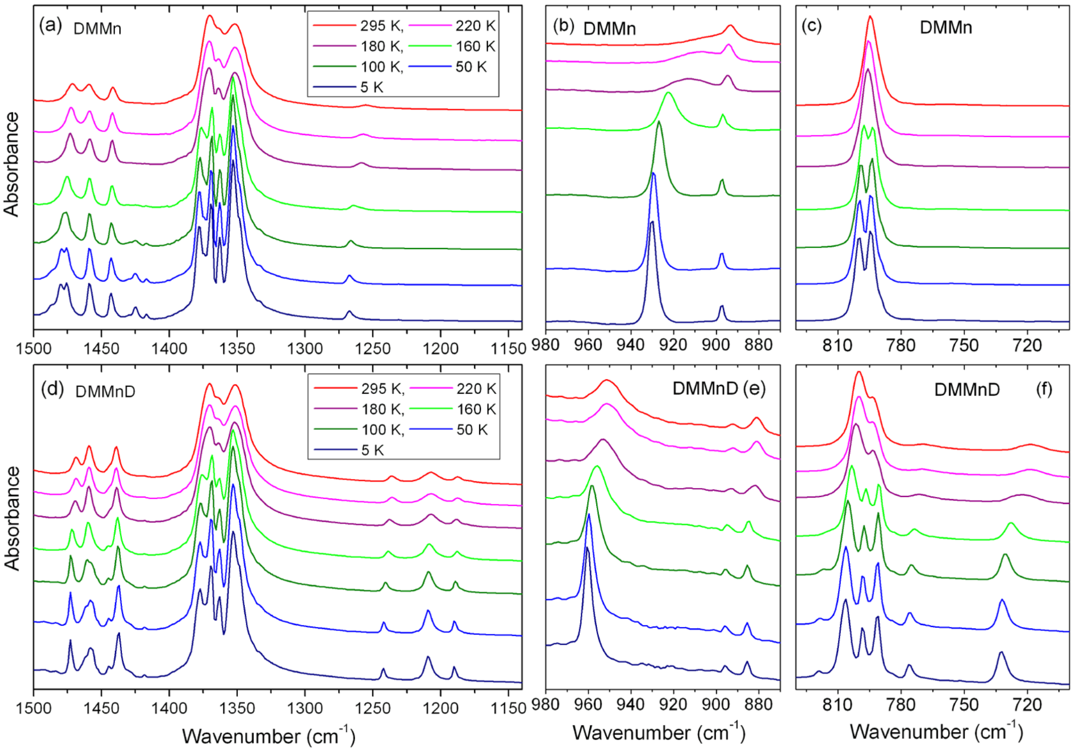

Figure 8. Detail of the IR spectra results corresponding to the spectral ranges 1140−1500, 870−980, and 700−830 cm^{-1} for DMMn (a, b, and c) and DMMnD (d, e, and f).

observed at about 814 and 810 cm^{-1} for DMNi exhibit upshifts of nearly 3.5 and 2 cm^{-1}, respectively, for DMNiD. The additional bands and upshifts may arise due to some resonance effects and/or coupling of the ν_3(HCOO$^-$) modes with other low frequency modes.

Nearly all bands observed below 370 cm^{-1} can be attributed to the lattice modes. Translational (T′) and librational (L) modes of the formate groups were typically observed below 250 cm^{-1},[23] whereas translational motions of the Mn^{2+} and Ni^{2+} cations usually contribute to the modes observed in the 150−

350 cm^{-1} region.[24] Study of DMA complexes with inorganic anions showed that lattice modes related to the DMA$^+$ cations should appear below 200 cm^{-1}.[22] Although the detailed assignment of the observed bands to T′ and L modes was not proposed, we may obtain some information on the location of these modes by comparison of DMA$^+$ with NH_4^+ cations. In the latter case, T′ and L modes were observed in the frequency region of 170−270 and 300−380 cm^{-1}, respectively.[25] Since in the NH_4^+ cation the two H-atoms are replaced by bulky CH_3 groups, one can expect a significant shift of T′(DMA) and L(DMA) modes toward lower frequencies. Moreover, lattice modes of DMA$^+$ should exhibit a slight shift toward lower frequencies upon deuteration. Our Raman and IR spectra show that weak shifts toward lower frequencies upon deuteration are observed for the bands located in the 130−170 cm^{-1} region and below 122 cm^{-1} (Figures S9 and S10, Tables S3 and S4, Supporting Information). We assign, therefore, these bands to L(DMA) and T′(DMA) modes, respectively.

Tables S3 and S4 show that the most significantly affected modes by the change of Mn^{2+} into Ni^{2+} are those assigned to carboxylate unit (ν_2, ν_3, and ν_4 modes). This result indicates that replacement of larger Mn^{2+} by smaller Ni^{2+} leads to significant changes in the C−O bonds and O−C−O bond angles; i.e., it affects significantly the anionic framework. The other modes are less affected, but one can notice that all modes related to the DMA$^+$ cation also exhibit noticeable shifts toward higher frequencies when Ni^{2+} replaces Mn^{2+}. This effect can be attributed to the smaller size of the cavity occupied by DMA$^+$ in the latter case.

Let us now discuss shortly the H-bond strength and isotopic effect. When no H-bonds are formed, the N−H and N−D stretching vibrations appear in the region 3300−3500 and 2400−2600 cm^{-1}, respectively (the frequency isotopic ratio ν(N−H)/ν(N−D) is close to 1.41).[22,26] When H-bonds are formed, the stretching modes usually shift toward lower frequencies, the corresponding bands become broader and more intense, and the isotopic ratio decreases even to about 1 for strong H-bonds.[27,28] In contrast to the stretching mode, the out-of-plane rocking mode should exhibit increase in frequency with increasing strength of the H-bond.[27] Our spectra show the N−H (N−D) stretching modes in the region 2790−3030 cm^{-1} (2080−2280 cm^{-1}) (see Tables S3 and S4); that is, these bands are shifted toward lower frequencies by 300−400 cm^{-1} (relatively to stretching frequencies of N−H and N−D bonds not involved in formation of H-bonds), and the frequency isotopic ratio is about 1.34. The observed shifts and value of the isotopic ratio indicate that the N−H···O H-bonds in the studied compounds are of medium strength. The comparison of the IR spectra show that the $\nu(NH_2)$ and $\rho(NH_2)$ modes shift to higher and lower wavenumbers, respectively, when Mn is replaced by Ni in the MOFs studied here (see Table S3, Supporting Information). This result indicates that the strength of H-bonds is slightly larger for DMNi, when compared to DMMn.

Temperature-Dependent Raman and IR Studies, and Mechanism of the Phase Transition. Temperature-dependent Raman and IR studies show that when temperature decreases below T_c, many of the Raman and IR bands split into a few components. It can also be noticed that many new bands appear at low temperatures, especially in the low frequency region below 400 cm^{-1}. According to the correlation diagram presented in Table S2, Supporting Information, due to decrease of symmetry from $R\bar{3}c$ to Cc below T_c, splitting is expected for the E_u and E_g modes of the metal-formate framework as well as $\nu_{as}(CH_3)$, $\delta_{as}(CH_3)$, and $\tau(CH_3)$ modes. Moreover, all modes that are only Raman-active or only IR-active as well as all silent modes should become both IR- and Raman-active in the low-temperature phase. This should lead to the appearance of new bands in the IR and Raman spectra below T_c. On the other hand, the modes of the NH_2 and CNC groups may be observed as single bands in the Cc phase if the Davydov splitting between the A′ and A″ components is negligible. This behavior is well reflected in the IR and Raman spectra; that is, the temperature-dependent Raman and IR spectra are consistent with the proposed symmetry change from $R\bar{3}c$ to Cc.

Decreasing of temperature leads also to significant changes in intensity of some bands and their full width at half-maximum (FWHM). Especially interesting changes are observed for the bands attributed to the N−H or N−D stretching modes, which appear in the region 2790−3030 cm^{-1} and 2080−2280 cm^{-1}, respectively. First, when the temperature is lowered, the bands become much sharper. Detailed temperature behavior of the 2087 cm^{-1} Raman band of DMMnD reveals that upon cooling the FWHM of this band exhibits a very pronounced discontinuous decrease at T_c (Figure 9). This behavior proves that the phase transition has strong first-order character. Second, they generally soften with a decrease in temperature (Figures S6 and S7, Supporting Information). Third, some of the N−D and N−H stretching modes exhibit a pronounced increase in intensity upon cooling (Figures 7, 9, S5−S7). The observed changes indicate that the phase transition is accompanied by significant changes in H-bonds. In particular, a shift toward lower frequencies and an increase in intensity indicate an increase of the H-bond strength with decreasing temperature. On the other hand, the strong decrease in FWHM reflects the highly dynamic nature of H-bonds in the high-temperature phase and provides evidence for proton (deuteron) ordering in the N−H···O (N−D···O) bonds at low temperatures. Figure 9 also shows that the intensity and frequency of the 2087 cm^{-1} mode exhibit a continuous increase upon cooling the low-temperature phase down to 5 K, without any clear saturation (Figure 9). This result indicates that H-bond strength increases in a continuous way upon cooling the low-temperature phase. FWHM of the discussed band exhibits a further pronounced decrease upon cooling the low-temperature phase. This result can be most likely attributed to strong anharmonicity of the H-bonds and incomplete ordering of

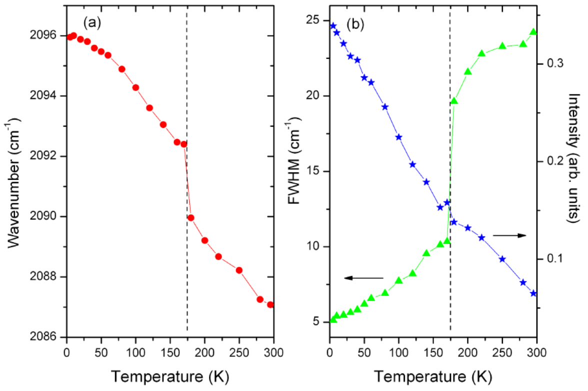

Figure 9. Temperature dependence of (a) mode frequency and (b) FWHM and intensity of the 2087 cm^{-1} Raman band of DMMnD corresponding to the $\nu(ND_2)$ mode. Solid lines are to guide the eye.

deuterons in the low-temperature phase near T_c. Here it is important to mention that ^{1}H NMR measurements of $[(CH_3)_2NH_2][Zn(HCOO)_3]$ suggested continuity of the proton motions through the phase transition.[8] Our results clearly show discontinuity of the deuteron motions through the phase transition, as evidenced by an abrupt change in FWHM of the $\nu(ND_2)$ mode at 2087 cm^{-1} near T_c (Figure 9). This difference can be attributed to a faster time scale of vibrational spectroscopy when compared to NMR. Therefore, though the deuteron or proton motions do not freeze at the NMR time scale, they freeze at the Raman or IR time scale.

In order to further explain the dynamics driving the phase transition, we also present the temperature dependence of a few selected vibrational frequencies and FWHM values for different molecular subunits of the studied compounds (Figures 10, 11 and S11−S14). Figure 10 represents the temperature evolution of $\nu_{as}(CNC)$ and $\nu_s(CNC)$ modes. The $\nu_{as}(CNC)$ modes exhibit a very clear upshift at T_c by about 3 cm^{-1}. Similar upshifts at T_c are also observed for the $\nu_s(CNC)$ modes. However, these upshifts are smaller for DMMn and DMNi (about 2 cm^{-1}) than DMMnD and DMNiD (nearly 3 cm^{-1}). These modes also exhibit pronounced decrease in FWHM around T_c (Figure 10c). Even more pronounced temperature evolution is observed for the $\rho(NH_2)$ and $\rho(ND_2)$ modes (Figure 11). These modes exhibit a very large FWHM at room temperature, that is, near 24−26 cm^{-1} for DMMn and DMNi and around 16 cm^{-1} for DMMnD and DMNiD. Smaller widths for the deuterated samples can be attributed to a reduced mean amplitude of vibration of the deuterium atom when compared to the hydrogen atom. With the lowering in the temperature, the FWHMs weakly decrease until T_c and then exhibit an abrupt decrease around T_c, followed by a continuous decrease in the low-temperature phase (Figure 11). The frequencies gradually increase, and at T_c an abrupt and pronounced upshift up to 10 cm^{-1} is observed for all samples. The observed temperature dependence of the discussed modes proves that the phase transition in the studied compounds has an order−disorder character and is governed by dynamics of the DMA^+ cations. The band broadening in molecular crystals is mainly due to anharmonicity and reorientation of molecules or ions. When dynamic disorder prevails over the phonon decay process, the width of a band is usually defined as

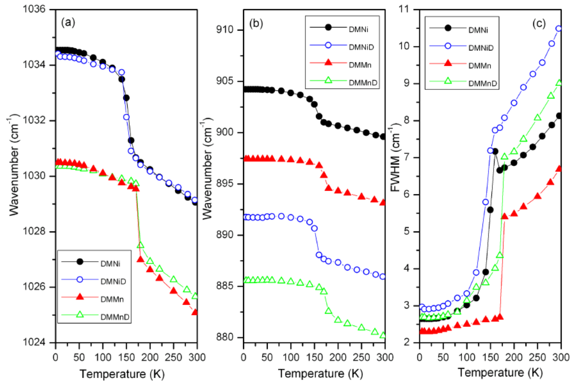

Figure 10. Temperature evolution of (a) $\nu_{as}(CNC)$ and (b) $\nu_s(CNC)$ mode IR frequencies of all samples. (c) FWHM of the respective modes. Solid lines are to guide the eye.

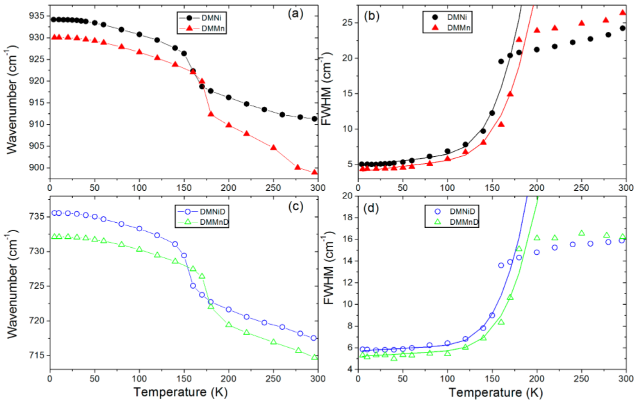

Figure 11. Temperature dependence of (a) $\rho(NH_2)$ and (c) $\rho(ND_2)$ IR mode frequencies as well as (b and d) FWHM of the respective modes of all samples. Solid lines in (a) and (c) are to guide the eye. Solid lines in (b) and (d) are fits on the data to eq 3.

$$\mathrm{FWHM} = A + BT + C\exp(-E_a/kT) \tag{3}$$

where E_a is the activation energy, k is the Boltzmann constant, and T is the temperature.[29] The constant A accounts for the broadening arising from factors other than the phonon decay, such as structural and compositional defects. The second and third term of eq 3 represents the influence of anharmonicity and thermally activated reorientational processes, respectively. Equation 3 enables us to determine the activation energy of reorientational processes for DMA^+ cation in the studied compounds using temperature dependence of the FWHM for the $\rho(NH_2)$ and $\rho(ND_2)$ IR-active modes (Figure 11). The fit on the data to eq 3 gives $A = 4.0$ cm^{-1}, $B = 0.015$ cm^{-1} K^{-1}, and $E_a = 97$ meV (9.36 KJ/mol) for DMMn; $A = 4.8$ cm^{-1}, $B = 0.015$ cm^{-1} K^{-1}, and $E_a = 92$ meV (8.88 KJ/mol) for DMNi; $A = 5.2$ cm^{-1}, $B = 0.005$ cm^{-1} K^{-1}, and $E_a = 103$ meV (9.94 KJ/mol) for DMMnD, and $A = 5.7$ cm^{-1}, $B = 0.005$ cm^{-1} K^{-1}, and $E_a = 98$ meV (9.46 KJ/mol) for DMNiD. These data show that the linear terms (B values) are significantly lower for the deuterated samples, implying smaller anharmonic contribution. They also show that the activation energy increases upon deuteration and when Mn replaces Ni. The values of the potential barrier estimated by us can be compared to those obtained for other compounds containing DMA^+ cations. For example, E_a was 0.19 eV for $[(CH_3)_2NH_2]_3[Bi_2Cl_9]$ and 0.1 eV for $[(CH_3)_2NH_2]_3[Sb_2Cl_9]$.[22] It is worth noting that the values obtained by us for DMMn (97 meV) and DMNi (92 meV) are close to the activation energy associated with the main spin−lattice relaxation path in $[(CH_3)_2NH_2][Zn(HCOO)_3]$, which was found to be 88 meV (8.5 KJ/mol).[8] It is also worth mentioning that our analysis indicates that the contribution of the reorientational processes to the observed broadening becomes important above about 100 K, whereas below 100 K this contribution becomes negligible and the observed changes in FWHM are related to the anharmonicity.

Let us now discuss briefly temperature-dependent changes of the anionic framework. Figure S1, Supporting Information1 shows that with a decrease in temperature from 295 K approaching the phase transition temperature T_c, the $\nu_3(HCOO^-)$ modes (the symmetric O−C−O bending modes) of DMNi and DMMn exhibit increase in the frequency up to 1.5 cm^{-1}, except of the 792 cm^{-1} mode of DMMn, which exhibits a decrease in the frequency by about 1.1 cm^{-1}. The deuterated samples, DMMnD and DMNiD, exhibit similar behavior, but the observed changes in the frequencies are slightly larger, up to 2.4 cm^{-1} for the 793 cm^{-1} mode of

DMMnD. The discussed bands exhibit also a very clear decrease of FWHM at T_c. It is worth noting that the observed changes in FWHM are significantly larger for the deuterated samples (Figure S11). The temperature evolution of $\nu_6(HCOO^-)$ Raman modes (C−H out-of-plane bending modes), presented in Figure S12, Supporting Information, shows that the behavior of these modes is very similar for DMMn and DMMnD. Frequencies of these modes change slightly with temperature down to T_c, but very significant shifts of these modes toward higher frequency are observed below T_c. Significant frequency shifts are also observed for the $\nu_1(HCOO^-)$ Raman modes (C−H stretching modes), observed in the 2820−2880 cm^{-1} range (see Figure S12). These changes are accompanied by a very clear and abrupt decrease of FWHM. Although the bands related to internal modes of $HCOO^-$ exhibit weaker changes than those related to DMA^+ cation, their temperature dependence indicates that the phase transition is also associated with distortion of the metal-formate framework. Since modes corresponding to vibrations of the C−H group of the formate ion exhibit much larger changes at T_c than the C−O vibrations, the C−H bonds are more significantly affected by the phase transformation than the C−O bonds. Another interesting observation is that larger anomalies are observed for $\nu_3(HCOO^-)$ and $\nu_s(CNC)$ modes of DMMnD and DMNiD when compared to similar modes of DMMn and DMNi. This result indicates that deuteration leads to larger lattice distortion at T_c. The larger lattice distortion suggests that deuteration leads to an increase of the interionic interaction between the DMA^+ cation and the metal-formate framework; that is, deuteration leads to an increase in the H-bond strength. According to Li et al. for a medium strength H-bond, as in our case, a negative Ubbelohde effect can be expected, that is, a shortening of the N···O distances (increase of H-bond strength) upon replacing H with D.[19] Thus our results are consistent with the correlation proposed by Li et al.[19] Here it is worth noting that in hydrogen-bonded crystals with order−disorder type phase transitions T_c decreases upon compression, and the pressure dependence of T_c is determined by the pressure change of the H-bond structure.[30] It has been shown that T_c decreases with a decrease in the length of the H-bond.[30] This correlation explains the significant decrease of T_c upon replacing larger Mn^{2+} ions with smaller Ni^{2+} ions in our samples. The observed downward shift of T_c for DMNiD when compared to DMNi is also consistent with shortening of the N···O distances upon deuteration. In the case of DMMn and DMMnD, the situation is less clear. The observation of a larger lattice distortion for DMMnD suggests an increase of the H-bond strength, while X-ray diffraction suggests a slightly weaker H-bond and T_c exhibits negligible change after deuteration. We suppose, therefore, that not only the N···O distance but also some other factors, for instance, electronegativity of the elements, affect T_c and the mechanism of the ferroelectric transition.

Figure S13 represents the temperature evolution of $\delta_{as}(CH_3)$ modes. Frequencies of the IR bands of DMMn (DMNi) at 1441 and 1459 cm^{-1} (1443 and 1460 cm^{-1}) do not show any clear anomalies at T_c. A clear upshift at T_c by about 4.8 cm^{-1} (4.0 cm^{-1}) is, however, observed for the 1472 cm^{-1} (1475 cm^{-1}) mode of DMMn (DMNi). The latter mode also exhibits clear splitting in the low-temperature phase. FWHMs of the discussed bands decrease continuously with decreasing temperature, showing no or weak anomalies near T_c (see Figure S13). The $\nu_{as}(CH_3)$ modes exhibit clear downshifts at T_c (Figure S14, Supporting Information), sugesting a decrease of the C−H bond lengths upon cooling. Figure S14 also shows that frequencies of the discussed modes and their temperature evolution are the same for DMMn and DMMnD samples within experimental error. In contrast to this behavior, a much more pronounced downshift is observed for the $\nu_s(CH_3)$ mode of DMMnD at 2972 cm^{-1} (1.8 cm^{-1}) than DMMn (only about 1.1 cm^{-1}). FWHMs of the discussed modes exhibit an abrupt but weak decrease by less than 1.6 cm^{-1} at T_c. It is worth noting that ^1H NMR measurements of $[(CH_3)_2NH_2][Zn(HCOO)_3]$ suggested that the methyl groups exhibit internal rotations around their 3-fold symmetry axes, and this rotation freezes only below 40 K.[8] Freezing of the internal rotation of the methyl groups leads to the appearance of a glassy state below 40 K.[8] Our results show a fast decrease in FWHM in the 295−5 K range for $\delta_{as}(CH_3)$ and $\nu(CH_3)$ modes of the studied compounds with negligible or small changes near T_c (Figures S13 and S14). This behavior can be attributed to fast slowing down of the internal rotation of the methyl group. However, we do not see any anomalies below 100 K in the temperature dependence of FWHM that could indicate the presence of a glassy state in the MOFs studied here.

Since these compounds exhibit magnetic ordering, spin−phonon coupling is expected that should lead to some subtle anomalies in the temperature evolution of phonon frequencies below T_N. Taking into account the exchange interactions between the magnetic atoms located at the nearest-neighboring sites only, for a displacement by x from the equilibrium position, the crystal potential U can be given by[31]

$$U = \frac{1}{2}kx^2 + \sum_{ij} J_{ij}(x)\langle S_i S_j\rangle \tag{4}$$

Here k, J_{ij}, and $<S_iS_j>$ is the force constant, exchange energy constant, and spin correlation function, respectively. Its second derivative

$$\frac{\partial^2 U}{\partial x^2} = k + \sum_{ij} \frac{\partial^2 J_{ij}}{\partial x^2}\langle S_i S_j\rangle \tag{5}$$

gives the harmonic force constant. Equation 5 shows that due to spin−phonon coupling the force constant has an additional contribution (second term). As a result, the phonon wavenumber is also affected by an additional contribution:[31]

$$\nabla\omega_i \equiv \lambda\langle S_i S_j\rangle \tag{6}$$

where the spin−phonon coupling constant λ is different for different phonons and can have either a positive or a negative sign. In general, one could expect significant changes for phonons, which involve motions that modulate spin exchange coupling. Since in the MOFs studied here the indirect magnetic exchange occurs through the formate ligands,[32] one may expect to observe some anomalies for the modes involving vibrations of the carboxylate group. Close inspection of our data reveal no anomalies for the modes related to DMA^+ cations. We can see, however, some weak anomalies for the $\nu_3(HCOO^-)$ modes (see Figure 12). In particular, this figure shows that for the Mn compounds frequency increases down to 20 K. At 10 K, it is practically the same as at 20 K, but a weak decrease is observed at 5 K. In the case of the Ni compounds, the frequency increases down to 40 K and then slightly decreases below 35 K. Note that the behavior of Ni compounds is significantly different than that of Mn compounds, and the observed

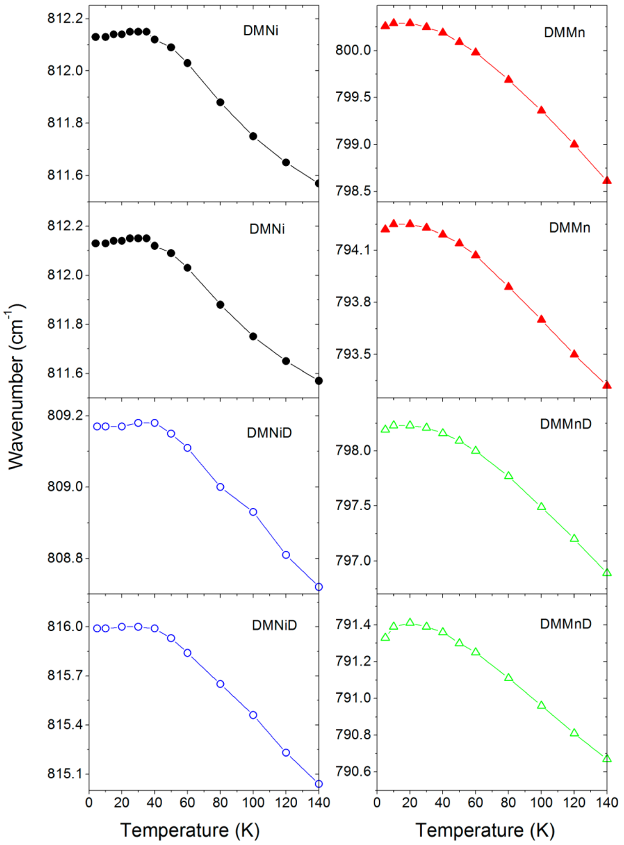

Figure 12. Temperature dependence of IR frequencies for the $\nu_3(HCOO^-)$ modes of the studied compounds below 140 K showing weak anomalies below 40 K due to spin-phonon coupling.

anomalies near 35 K for Ni compounds and below 10 K for Mn compounds correspond well with the onset of the magnetic order found at 37 K for DMNi and 8.5 for DMMn. This result proves that the weak anomalies can be attributed to spin−phonon coupling. It is worth adding that the observed downward frequency shifts from the expected behavior due to pure phonon−phonon anharmonic interactions are very small, less than 0.2 cm^{-1}, that is, much smaller than typically found in inorganic crystals exhibiting magnetic order at low temperatures. For instance, in the case of multiferroic $Mn_{0.93}Fe_{0.07}WO_4$ the largest shift due to spin-phonon coupling was about 1 cm^{-1}.[11]

■ CONCLUSIONS

Replacement of a hydrogen atom by a deuterium atom allowed locating all vibrational modes that involve strong contribution of hydrogen (deuterium) atom motions. In particular, it allowed for decoupling of N−D stretching modes from the stretching modes of the CH_3 and C−H groups. This in turn allowed observing clearly temperature-dependent changes in the N−D stretching modes region due to changes in the H-bond strength.

DSC, dielectric measurements, X-ray diffraction, and Raman and IR measurements have demonstrated that in the high-temperature paraelectric phase the DMA$^+$ cations are dynamically disordered, because the H-bonds between the NH_2 (ND_2) groups and the metal-formate framework are disordered. The decrease of temperature leads to an increase of the H-bonds strength and slowing down of the hopping motion of the DMA$^+$ cations. The slow dynamics of large DMA$^+$ cations is responsible for the observed pronounced dielectric dispersion. When the temperature reaches some critical value T_c, vibrational frequencies and FWHMs exhibit abrupt changes, indicating the onset of the first-order phase transition into the ferroelectric phase. Though our results provide evidence for ordering of DMA$^+$ cations below T_c due to the proton (deuteron) ordering in N−H···O (N−D···O) bonds, they also show that some amount of motion is retained by the DMA$^+$ cation in the ferroelectric phase, and a complete freezing-in of this motion occurs below 100 K. Our results also show that though the ferroelectric phase transition is mainly driven by ordering of DMA$^+$ cations, it is also accompanied by significant distortion of the metal-formate framework.

The low-temperature studies show that magnetic properties of the studied compounds can be explained assuming that they are ordered ferrimagnetically with nearly compensated magnetic moments of Ni and Mn. Our spectroscopic results do not provide any evidence for the appearance of a glassy state below 40 K in the studied crystals, as suggested for $[(CH_3)_2NH_2][Zn(HCOO)_3]$.[8] We observe, however, weak anomalies in the temperature dependence of vibrational frequencies below 40 K that appear due to spin−phonon coupling.

Finally, our results show that deuteration has some impact on the properties and mechanism of the phase transitions. In particular, our results show that deuteration leads to upshifts of some bands. Furthermore, more significant distortion of the metal-formate framework occurs at the paraelectric−ferroelectric phase transition for the deuterated samples. The observed differences in the behavior of DMMn and DMNi and their deuterated analogues can be most likely attributed to change of the H-bond strength after deuteration.

■ ASSOCIATED CONTENT

Supporting Information

X-ray crystallographic information files (CIF) for crystal structures of DMNi, DMNiD, DMMN, and DMMnD at 295 K. Figures S1−S14: Powder X-ray diffraction, DSC traces, real and imaginary parts of the complex dielectric constant, IR and Raman spectra, temperature dependence of bandwidths and frequencies. Tables S1−S4: X-ray data collection and refinement parameters, the correlation diagram showing the correspondence between the optical modes in the $R\bar{3}c$ and Cc structures, and Raman and IR frequencies for all samples at 295 and 5 K. This material is available free of charge via the Internet at http://pubs.acs.org.

■ AUTHOR INFORMATION

Corresponding Author

*E-mail: m.maczka@int.pan.wroc.pl; phone: +48-713954161; fax: +48-713441029.

Notes

The authors declare no competing financial interest.

■ ACKNOWLEDGMENTS

This research was supported by the National Center for Science (NCN) in Poland under project No. DEC-2011/03/B/ST5/01019.

■ REFERENCES

(1) (a) Fiebieg, M. *J. Phys. D: Appl. Phys.* **2005**, *38*, R123−R152. (b) Tokura, Y. *J. Magn. Magn. Mater.* **2007**, *310*, 1145−1150.

(2) Maczka, M.; Ptak, M.; Hermanowicz, K.; Majchrowski, A.; Pikul, A.; Hanuza, J. *Phys. Rev. B* **2011**, *83*, 174439.

(3) (a) Rogez, G.; Viart, N.; Drillon, M. *Angew. Chem., Int. Ed.* **2010**, *49*, 1921−1923. (b) Ramesh, R. *Nature* **2009**, *461*, 1218−1219.

(4) (a) Wang, Z.; Zhang, B.; Otsuka, T.; Inoue, K.; Kobayashi, H.; Kurmoo, M. *Dalton Trans.* **2004**, 2209−2216. (b) Wang, X. Y.; Gan, L.; Zhang, S. W; Gao, S. *Inorg. Chem.* **2004**, *43*, 4615−4625.

(5) (a) Jain, P.; Dalal, N. S.; Toby, B. H.; Kroto, H. W; Cheetham, A. K. *J. Am. Chem. Soc.* **2008**, *130*, 10450−10451. (b) Jain, P.; Ramachandran, V.; Clark, R. J.; Zhou, H. D.; Toby, B. H.; Dalal, N. S.; Kroto, H. W; Cheetham, A. K. *J. Am. Chem. Soc.* **2009**, *131*, 13625−1327. (c) Guo, M.; Cai, H. L.; Xiong, R. G. *Inorg. Chem. Commun.* **2010**, *13*, 1590−1598.

(6) Fu, D. W; Zhang, W.; Cai, H. L.; Zhang, Y.; Ge, J. Z.; Xiong, R. G.; Huang, S. D.; Nakamura, T. *Angew. Chem., Int. Ed.* **2011**, *50*, 11947−11951.

(7) Wang, W.; Yan, L.-Q.; Cong, J.-Z.; Zhao, Y.-L.; Wang, F.; Shen, S.-P.; Zhou, T.; Zhang, D.; Wang, S.-G.; Han, X.-F.; Sun, Y. *Sci. Rep.* **2013**, *3*, 2024.

(8) Besara, T.; Jain, P.; Dalal, N. S.; Kuhns, P. L.; Reyes, A. P.; Kroto, H. W; Cheetham, A. K. J. *Proc. Nat. Acad. Soc. U. S. A.* **2011**, *108*, 6828−6832.

(9) Pato-Doldan, B.; Sanchez-Andujar, M.; Gomez-Aguirre, L. C.; Yanez-Vilar, S.; Lopez-Beceiro, J.; Gracia-Fernandez, C.; Haghighirad, A. A.; Ritter, F.; Castro-Garcia, S.; Senaris-Rodrigues, M. A. *Phys. Chem. Chem. Phys.* **2012**, *14*, 8498−8501.

(10) Sanchez-Andujar Presedo, S.; Yanez-Vilar, S.; Castro-Garcia, S.; Shamir, J.; Senaris-Rodrigues, M. A. *Inorg. Chem.* **2010**, *49*, 1510−1516.

(11) Maczka, M.; Sanjuan, M. L.; Fuentes, A. F.; Macalik, L.; Hanuza, J.; Matsuhira, K.; Hiroi, Z. *Phys. Rev. B* **2009**, *79*, 214437.

(12) Merunka, D.; Rakvin, B. *Struct. Bonding (Berlin)* **2007**, *124*, 149−198.

(13) Syamaprasad, U.; Vallabhan, C. P. G. *Phys. Lett. A* **1982**, *89*, 37−40.

(14) Hidaka, T.; Oka, K. *Phys. Rev. B* **1990**, *42*, 8295−8304.

(15) Zhang, W.; Xiong, R. G. *Chem. Rev.* **2012**, *112*, 1163−1195.

(16) Petzelt, J.; Kamba, S. *Spectrosc. Prop. Inorg. Organomet. Compd.* **2009**, *40*, 49−71.

(17) Sobiestianskas, R.; Grigas, J.; Samulionis, V. *Phase Trans.* **1991**, *29*, 167−178.

(18) Kageyama, H.; Khomskii, D. I.; Levitin, D. Z.; Markina, M. M.; Okuyama, T.; Uchimoto, T.; Vasil'ev, A. N. *J. Magn. Magn. Mater.* **2003**, *262*, 445−451.

(19) Li, X. Z.; Walker, B.; Michaelides, A. *Proc. Nat. Acad. Soc. U. S. A.* **2011**, *108*, 6369−6373.

(20) (a) Maczka, M.; Hanuza, J.; Kaminskii, A. A. *J. Raman Spectrosc.* **2006**, *37*, 1257−1264. (b) Magalhaes, A. L.; Madail, S. R. R. S.; Ramos, M. J. *Theor. Chem. Acc.* **2000**, *105*, 68−76.

(21) Mylrajan, M.; Srinivasan, T. K. K. *J. Phys. Chem. Solids* **1998**, *8*, 929−937.

(22) (a) Samet, A.; Ben Ahmed, A.; Mlayah, A.; Boughzala, H.; Hlil, E. K.; Abid, Y. *J. Mol. Struct.* **2010**, *977*, 72−77. (b) Wojtaś, M.; Bator, G.; Baran, J. *Vibr. Spectrosc.* **2003**, *33*, 143−152.

(23) (a) Berger, J. *J. Phys. C* **1975**, *8*, 2903−2910. (b) Ayala, A. P.; Henriques Neto, J. M.; Paschoal, C. W. A.; Guedes, I.; Sasaki, J. M.; Freire, P. T. C.; Melo, F. E. A.; Medes Filho, J.; Leyva, A. G.; Polla, G.; Vega, D.; Perazzo, P. K. *J. Raman Spectrosc.* **2000**, *31*, 491−495. (c) Heyns, A. M. *J. Chem. Phys.* **1986**, *84*, 3610−3616.

(24) Ptak, M.; Maczka, M.; Gagor, A.; Pikul, A.; Macalik, L.; Hanuza, J. *J. Solid State Chem.* **2013**, *201*, 270−279.

(25) (a) Wang, C. H.; Wright, R. B. *J. Chem. Phys.* **1973**, *58*, 1411−1419. (b) Balusubramanian, M.; Ramakrishnan, V.; Rajendran, S. *Pramana - J. Phys.* **1991**, *36*, 603−610. (c) Samantaray, R.; Clark, R. J.; Choi, E. S.; Dalal, N. S. *J. Am. Chem. Soc.* **2012**, *134*, 15953−15962.

(26) Durig, J. R.; Bush, S. F.; Baglin, F. G. *J. Chem. Phys.* **1968**, *49*, 2106−2117.

(27) (a) Arunan, E.; Desiraju, G. R.; Klein, R. A.; Sadlej, J.; Scheiner, S.; Alkorta, I.; Clary, D. C.; Crabtree, R. H.; Dannenberg, J. J.; Hobza, P.; Kjaergaard, H. G.; Legon, A. C.; Mennucci, B.; Nesbitt, D. *Pure Appl. Chem.* **2011**, *83*, 1619−1636. (b) Jarmelo, S.; Reva, I.; Carey, P. R.; Fausto, R. *Vib. Spectrosc.* **2007**, *43*, 395−404.

(28) Sobczyk, L.; Obrzyd, M.; Filarowski, A. *Molecules* **2013**, *18*, 4467−4476.

(29) Carabatos-Nedelec, C.; Becker, P. *J. Raman Spectrosc.* **1997**, *28*, 663−671.

(30) Barabash, A. I. *J. Mol. Struct.* **1998**, *450*, 23−28.

(31) (a) Lee, J. I.; Noh, T. W.; Bae, J. S.; Yang, I. S.; Takeda, T.; Kanno, R. *Phys. Rev. B* **2004**, *69*, 214428. (b) Ptak, M.; Maczka, M.; Hermanowicz, K.; Pikul, A.; Hanuza, J. *J. Solid State Chem.* **2013**, *199*, 295−304.

(32) Baker, P. J.; Lancaster, T.; Franke, I.; Hayes, W.; Blundell, S. J.; Pratt, F. L.; Jain, P.; Wang, Z. M.; Kurmoo, M. *Phys. Rev. B* **2010**, *82*, 012407.